IOP Publishing Journal of Physics: Condensed Matter
J. Phys.: Condens. Matter **32** (2020) 195802 (8pp) https://doi.org/10.1088/1361-648X/ab6e42

Novel mechanism for weak magnetization with high Curie temperature observed in H-adsorption on graphene

J G Che

Surface Physics Laboratory (National Key Laboratory), Key Laboratory of Computational Physical Sciences (MOE), Department of Physics and Collaborative Innovation Center of Advanced Microstructures, Fudan University, Shanghai 200433, People's Republic of China

E-mail: jgche@fudan.edu.cn

Received 24 September 2019, revised 4 December 2019
Accepted for publication 21 January 2020
Published 13 February 2020

Abstract

To elucidate the physics associated with the magnetism observed in nominally nonmagnetic materials containing only *sp*-electrons, we have developed an extreme model to simulate the adsorption of H (in a straight-line form) on graphene. Our first principles calculations for the model result in a ferromagnetic ground state at a high temperature with a magnetic moment of one Bohr magneton per H atom. The removal of p_z-orbitals from sublattice B of graphene introduces p_z-vacancies. The p_z-vacancy-induced states are created not because of the variations in interatomic interactions but because of the p_z-orbital imbalance between two sublattices (A and B) of the conjugated p_z-orbital network. Therefore, some critical requirements should be satisfied to create these states (denoted as $p_z^{\text{imbalance}}$) to avoid further imbalances and to minimally affect the conjugated p_z-orbital network. The requirements for the creation of $p_z^{\text{imbalance}}$ can be given as follows: (1) $p_z^{\text{imbalance}}$ consists of p_z-orbitals of only the atoms in sublattice A, (2) the spatial wavefunction of $p_z^{\text{imbalance}}$ is antisymmetric, and (3) in principle, $p_z^{\text{imbalance}}$ extends over the entire crystal without decaying, unless other p_z-vacancies are encountered. Both the origin of spin polarization and the magnetic ordering of the model can be attributed to the aforementioned requirements.

Keywords: *sp*-electron magnetism, long-ranged magnetic ordering, pi-electron conjugated network

(Some figures may appear in colour only in the online journal)

1. Introduction

The magnetism in nominally nonmagnetic materials containing only *sp*-electrons is a popular research topic because of their potential practical importance [1–4]. Among the reported controversial experimental observations with respect to the nonmagnetic materials [5–8], the high Curie temperature under such weak magnetization (three or four orders of magnitude smaller than that for conventional magnets) is considerably confusing [9–15]. There is no appropriate methodology to explain the manner in which defect-induced magnetic moments (MMs) localized far away from each other (where the distance between MMs is related to the defect concentration) could be coupled in ferromagnetic (FM) ordering at a temperature greater than room temperature. Although calculation results consistently show that the *sp*-electrons are spin-polarized by defects [1, 16–20], a convincing description of the physics associated with this phenomenon has not yet been provided. Therefore, exploring the origin of this phenomenon has become an overwhelming challenge in materials science [4, 21].

Two serious difficulties are associated with the theoretical study of these materials. First, the origin of the spin polarization of the *sp*-electrons remains unexplained because Heisenberg established 90 years ago that the principle quantum number of electrons that contribute to magnetism

must be greater than or equal to three [22, 23]. Second, the major difficulty is that no current theories have convincingly explained the manner in which long-range localized MMs (on defect centers) can be coupled in FM ordering at such a high Curie temperature. There must be an unrecognized magnetic mechanism at work.

In our previous papers [24, 25], we showed that the spatial wavefunctions of the electronic states contributing to magnetism were antisymmetric, thereby dispelling the uncertainties associated with the spin polarization of the *sp*-electrons. To address the question of magnetic coupling, we proposed in our previous paper [24] that the p_z-orbital imbalance induced by vacancies would result in magnetic ordering in the material. However, it is computationally intensive to simulate graphene having a vacancy concentration sufficiently similar to that for which magnetism can be experimentally observed [12]. Therefore, we did not perform first principles calculations to compare the total energy difference between the FM and antiferromagnetic (AFM) ordering and only conducted an analysis that resulted in the abovementioned conclusions.

In a two-dimensional (2D) system, a point defect causes a resonance that decays with r (the distance from the defect) [24, 26–29], whereas according to perturbation theory [30], a defect that is periodically arranged infinitely throughout the 2D system can cause a resonance without any decay. In this paper, we develop an extreme model with respect to the adsorption of H (in a straight-line form) on graphene to robustly demonstrate that the FM (with a high Curie temperature) originates from the p_z-orbital imbalance between two graphene sublattices. Our objective is not to determine whether such an extreme model could be experimentally realized; instead, we intend to use the developed extreme model to understand the novel magnetic mechanism [24] that is at work in these materials.

2. Calculation methods

Our results were obtained using first principles calculations that were implemented using the VASP package [31] with a calculation setup similar to those used in our previous papers [24, 25], that is, the wavefunctions were expanded in a plane-wave basis set with an energy cutoff of 500 eV. The interaction between the atoms and electrons was described by the projector augmented plane-wave method [32]. The generalized gradient approximation [33] for exchange-correlation effects was used. The adsorption of H on graphene was simulated using a supercell in a 48 × 1-sized cell of the original graphene. The k-points were sampled in the 2D Brillouin zone using 4 × 48 meshes for the total energy calculations. The vacuum thickness was maintained larger than 20 Å. All the atoms were relaxed until the Hellmann–Feynman forces on the atoms were smaller than 0.02 eV Å^{-1}. This calculation setup was found to be sufficiently accurate for the purposes of our study. For example, the use of this calculation setup resulted in a calculated lattice constant of 1.42 Å for graphene, which is in good agreement with the experimental value [34].

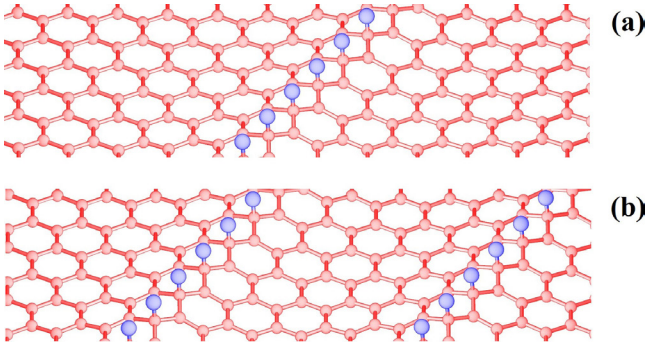

Figure 1. Perspective view of H-adsorption on one sublattice of graphene forming (a) one and (b) two H lines. Blue and red balls represent H and C atoms, respectively. In (b), two H lines are separated by six of the original graphene units.

3. Results and discussion

3.1. One H adsorption on graphene

The bonded crystals with only *sp*-electrons do not exhibit magnetism, as concluded by Heisenberg theory [22, 23]. However, magnetism induced by vacancies, nonmetal or alkaline-earth metal adatoms on graphene and graphite has been experimentally observed above room temperature and predicted by calculations [1, 2, 21, 35–37]. However, a convincing theory that can explain these phenomena is still required [2, 19, 21, 35, 38–41]. Previously, we have also explained [24, 25] why Hund's rule does not hold when interpreting calculation results based on singlet-electron approximation and the Bloch theorem in band theory.

In a previous study [24], we proposed that the p_z^*-nonbonding states (referred to as the zero-mode in literature [26, 42]) play a critical role in both the spin polarization of *sp*-electrons and the magnetic coupling in graphene containing vacancies. As mentioned in the Introduction, an extreme model has been developed in this study to simulate H-adsorption (in a straight-line form) on graphene, as shown in figure 1(a). Instead of introducing a C-vacancy by removing a C atom from graphene, we have introduced a p_z-vacancy in graphene via the H saturation of a p_z-orbital of C located below H (denoted as C_H). This model enables us to avoid cutting off graphene (if the vacancies form in a straight line) while excluding antibonding states (induced by the interactions among the three dangling bonds caused by the vacancy). The model enables us to focus only on the p_z-vacancy-induced states. Considering our computational resources, we adopt a supercell of a 48 × 1-sized graphene to observe the long-range nature of the resonance states and examine the MM coupling in the model.

The C($2s^2 2p^2$) atom in graphene prefers to hybridize in one p_z and three sp^2 orbitals (where the z-axis is perpendicular to the graphene plane) [34]. The sp^2-orbitals form σ-bonds as a backbone of the honeycomb lattice comprising two sublattices denoted as A and B. Each of the atoms in sublattice A has three neighboring atoms in sublattice B and vice versa. The p_z-orbital and three sp^2-orbitals in graphene are orthogonal;

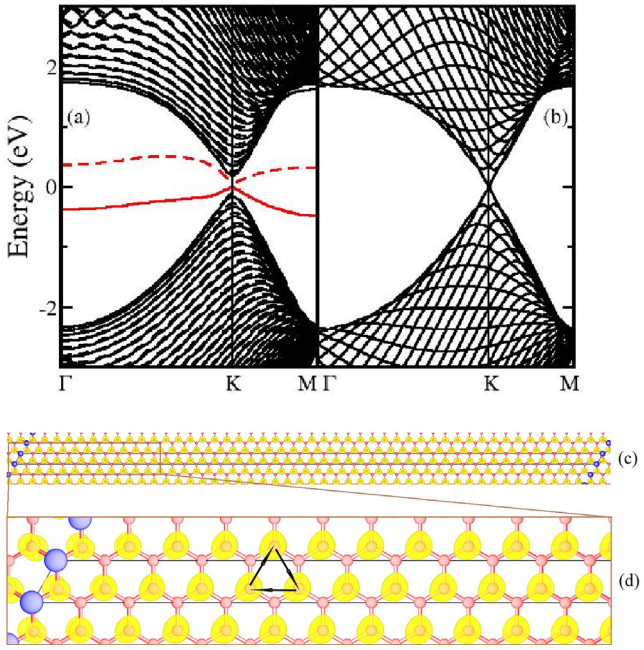

Figure 2. Band structures of a 48 × 1-sized graphene (a) with and (b) without H-adsorption, where the solid and dashed curves represent majority and minority states, respectively. K (0, 1/3) with $\mathbf{b}_1$ and $\mathbf{b}_2$ as units is folded from the K-point of the original graphene, and the Fermi level is set to zero. (c) Charge distribution of the solid red band in (a) at the K-point. (d) Enlargement of the brown rectangular portion in (c). Thick lines in (c) and (d) represent the 2D boundary of the supercell, red and blue balls in (c) and (d) represent C and H atoms, respectively, and the yellow regions show the charge distribution for the red state at the K-point in (a). Angles between arrows in (d) show the phase difference between the two respective atoms.

hence, they do not interact with each other. Therefore, the p_z-orbitals (p_z-electrons) over the two sublattices under C_{3V} symmetry coherently form a conjugated p_z-orbital (p_z-electrons) network, which is critical for obtaining magnetism in graphene.

Figure 1(a) shows the atomic configuration of the supercell for the adsorption of one H atom onto the 48 × 1-sized graphene with unit vectors, $\mathbf{a}_1 = 48(\sqrt{3/2}, -1/2)a$ and $\mathbf{a}_1 = 48(\sqrt{3/2}, 1/2)a$. C_H has three carbon atoms as its nearest neighbors. However, only two of the three carbon atoms could be present in the supercell because of the period along $\mathbf{a}_2$. The optimized atomic structure shows that the adsorption of H caused C_H to rise 0.68 Å above the graphene plane, whereas the two nearest neighbors of the H atom were 0.34 and 0.26 Å above the graphene plane. The distances between C_H and its two nearest neighbors were 1.48 and 1.52 Å. For comparison, the corresponding value in perfect graphene is 1.42 Å [34]. Clearly, C_H transformed from sp^2 hybridization in graphene to sp^3 hybridization after the adsorption of H, and its p_z-orbital (dangling bond) was saturated as expected, resulting in a p_z-vacancy, that is, there was a p_z-orbital imbalance between the two sublattices. Except for the aforementioned changes, there were no other changes in the C–C bond lengths that were larger or smaller than 0.04 Å relative to those in perfect graphene.

To determine the origin of the magnetism, the band structures of the ground state of the 48 × 1-sized graphene with and without the adsorption of H are presented in figures 2(a) and (b), respectively. By comparing the two band structures, two features can be clearly observed after the adsorption of H on the 48 × 1-sized graphene. First, the degeneration at the Dirac-point of graphene, as shown in figure 2(b), was lifted after the adsorption of H, resulting in a gap of approximately 0.3 eV. Second, the red (solid and dashed) bands in figure 2(a) exhibit spin-splitting from 0.1 to 0.9 eV along 2D-BZ. The graphene with a p_z-vacancy was thus semiconducting with a gap of 0.1 eV. The majority (solid) red band was fully occupied, and the minority (dashed) red band was empty, contributing 1 μ_B per H to the MM. Figure 2(b) clearly shows the folded structure of the original graphene band obtained from a 48-folded 2D-BZ.

In previous studies [15–18, 28], the H atom was considered as a point-defect adsorption on graphene, and the induced 1 μ_B per H was ascribed to Hund's rule because the induced electronic states appeared to be considerably localized. However, as discussed in our previous papers [24, 25], caution is required when using first principles calculations based on band theory because all the electrons in the band theory extend over the entire crystal as per the Bloch theorem, even if the bands appear to be flat [43].

To examine the nature of the majority red band, we calculated the charge distribution of the majority red band at the K-point, shown in figures 2(c) and (d). At first glance, the electrons were distributed on each atom in sublattice A with almost the same isosurfaces, indicating that the red state extended over the entire supercell without decaying, as expected. This extending nature motivated us to study straight-line defects in graphene instead of point defects. In fact, the electron distribution on sublattice A indicated an important feature: the spatial wavefunction of the state should be antisymmetric. That is, the phases of the wavefunction components on the two neighboring atoms belonging to sublattice A should be antisymmetric. Otherwise, electrons would accumulate on the atom (sublattice B) between the two neighboring atoms (sublattice A), resulting in an extra imbalance. This is impossible. Note that the length of the 48 × 1-sized supercell was already 120 Å. In principle, a consequence of the antisymmetric wavefunction is that the state should extend infinitely. Otherwise, terminating the wavefunction at one point will create an additional imbalance without any wavefunction at the opposite side of the broken point.

Although the red state in figure 2(a) was an H-induced state, its wavefunction was not localized but extended over the entire supercell and comprised p_z-orbitals of only the atoms in sublattice A. Note that the atoms in sublattice A belonged to the second nearest neighbors [34]. Therefore, the state was not caused by a change in the localized atomic interaction due to H-adsorption, but was created as a response of the conjugated p_z-electron network to a p_z-electron imbalance between the two sublattices.

In our previous paper [24], we used 'nonbonding state (p_z^*)' to describe the involved state following molecular orbital theory from quantum chemistry. However, imbalance is more essential than nonbonding with respect to the inherent nature of this state. In the absence of a suitable name, we temporarily

Table 1. Total energy (eV) per supercell for FM and AFM of two H separated by units (N). $\Delta E = E(\mathrm{AFM}) - E(\mathrm{FM})$.

N	3	6	12	18	24
E(FM)	−889.365	−889.427	−889.419	−889.422	−889.427
E(AFM)	−889.338	−889.404	−889.398	−889.400	−889.405
ΔE	0.027	0.022	0.022	0.022	0.022

refer to this state as an imbalanced state (denoted as $p_z^{\mathrm{imbalance}}$) for the purposes of discussion in the following section, to distinguish it from the lone pair state of the dangling bond, which is referred to as a nonbonding state in literature.

Because the induced state was caused by the p_z-electron imbalance, the response of the conjugated p_z-electron network to the imbalance should not create any further imbalance and should minimally affect the conjugated p_z-electron network. When one p_z-electron in sublattice A loses its pairing in sublattice B, the imbalance could be rectified by filling the induced state with one p_z-electron in sublattice A. However, if one p_z-electron was provided by one C atom in sublattice A (denoted by C_A) near the p_z-vacancy, this response would be electrostatically unstable and break its pairing with the atom in sublattice B near C_A. Thus, unpairing would continue indefinitely and alternatively appear on the both sublattices. Therefore, to minimally affect the conjugated p_z-electron network, each atom in sublattice A approximately provided $1/N_A$ electrons to form the $p_z^{\mathrm{imbalance}}$ state, where N_A denotes the number of atoms in sublattice A in a supercell.

Therefore, rectifying the imbalance involved the following conditions: (1) $p_z^{\mathrm{imbalance}}$ should comprise p_z-orbitals of only the atoms in sublattice A, (2) the $p_z^{\mathrm{imbalance}}$ wavefunction should be antisymmetric, and (3) $p_z^{\mathrm{imbalance}}$ should extend infinitely over the entire crystal without decaying. The electron antisymmetric exchange principle [44] states that the spin wavefunction of $p_z^{\mathrm{imbalance}}$ should be symmetric. This is the origin of the MMs caused by the *sp*-electrons in this material. That is, the MMs originate from the response of the conjugated p_z-electron network to the p_z-electron imbalance between two sublattices.

By counting the number of electrons within the supercell, only one electron filled $p_z^{\mathrm{imbalance}}$ and was distributed over all the 48 atoms of sublattice A of the entire supercell, contributing 1 μ_B per H. Based on the isosurfaces shown in figures 2(b) and (c), we concluded that the charge distribution on these atoms was approximately identical. That is, a contribution of 1/48 μ_B was obtained from each atom of sublattice A in the supercell. Note that these MMs were not atomic MMs isolated on atoms but were inherently parallel on the atoms because the MMs were the collective contribution from one electronic state. This result explains why such weak MMs with only 1 μ_B and in parallel alignment could be distributed over the entire supercell.

Here, we should explain the implications of an antisymmetric wavefunction for the supercell, as shown in figure 1(a). There was a phase difference of $e^{-i2\pi/3}$ between the neighboring atoms in sublattice A. The angle between $\mathbf{a}_2$ and $\mathbf{a}_1$ was $2\pi/3$. Each arrow in figure 2(d) represents a phase factor of $e^{-i2\pi/3}$ between the two atoms. Thus, an antisymmetric wavefunction indicates that the sum of the p_z-orbital components of the three atoms surrounding any atom in sublattice B was zero (within an accuracy of 10^{-6}), thereby ensuring the absence of orbital components for $p_z^{\mathrm{imbalance}}$ on sublattice B.

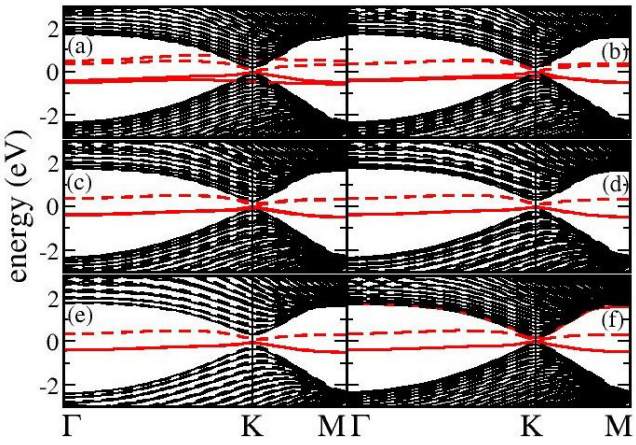

Figure 3. Same caption as that for figure 2(a), except for band structures of the 48 × 1-sized graphene with two adsorbed H that are separated by (a) 3, (b) 6, (c) 12, (d) 18, and (e) 24 units; (f) is the same as figure 2(a) and serves as a comparison.

3.2. Two H adsorption on graphene

A single p_z-vacancy in sublattice B created $p_z^{\mathrm{imbalance}}$, which was the response of the conjugated p_z-electron network to a p_z-electron imbalance between two sublattices. How did the conjugated p_z-electron network respond to the simultaneous presence of two p_z-vacancies in sublattice B? More p_z-electrons in sublattice A were required to rectify the imbalance caused by increasing the number of p_z-vacancies in sublattice B because $p_z^{\mathrm{imbalance}}$ was not created by a change in localized atomic interactions but by the p_z-electron imbalance. Therefore, changing calculation method [45, 46] for the interatomic interaction cannot change the magnetism induced by the imbalance states. In this case, the requirements (i.e. no additional imbalance and minimization of the effect on the conjugated p_z-electron network) of $p_z^{\mathrm{imbalance}}$ resulted in only a recombination of the p_z-orbitals of sublattice A.

The above conclusion was obtained by considering two p_z-vacancies on sublattice B separated by different units (N). The atomic configuration of two H atoms on one sublattice ($N = 6$) is shown in figure 1(b). The configurations were similar for $N = 3$, 6, 12, 18, and 24. Table 1 lists the total energies of FM and AFM for different N values. From the table, FM was energetically more favorable than AFM by at least 220 meV. Note that by placing H 5 Å above the graphene plane and calculating the total energy, the obtained energy for the

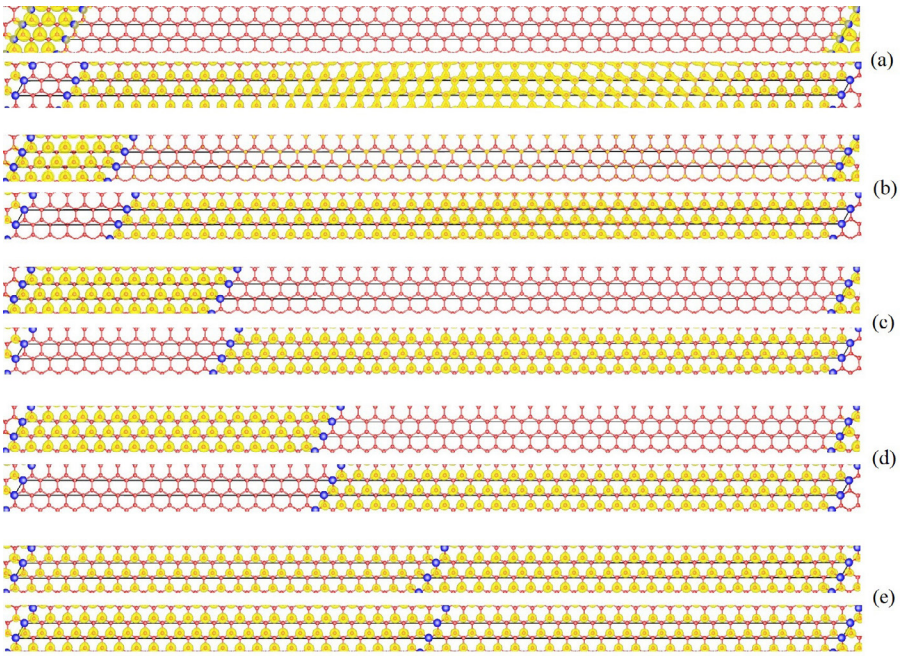

Figure 4. Charge distribution of two occupied states that correspond to the red bands at the K-point in figures 3(a)–(e). One H atom is adsorbed on unit 0 of the 48 × 1-sized graphene, and (a)–(e) correspond to the other H atom adsorbed on units 3, 6, 12, 18, and 24, respectively. Top and bottom subfigures in each panel correspond to imbalanced states with lower and higher energies, respectively. Red and blue balls represent C and H atoms, respectively, and thin solid lines represent the supercell boundary.

adsorption of H on graphene was estimated to be 1.033 eV. Because the current models for calculating the transition temperature are based on magnetic coupling (interaction parameters) between the nearest neighbors, they cannot be used in our case, where one MM contributed by one electronic state widely distributes as a whole moment on all the atoms of sublattice A (see below). However, we would point out that the energy difference of 220 meV between FM and AFM corresponds ($1\,\text{eV} = 1.160\,48 * 10^4$ K) to a temperature higher than 2500 K, in agreement with experimental observations of a high Curie temperature in proton-irradiated graphene. The MM for FM was 2 μ_B per supercell or 1 μ_B per H For all the five cases.

The band structures of the adsorption of two H atoms (separated by $N = 3$, 6, 12, 18, and 24 units) on one sublattice of the 48 × 1-sized graphene are plotted in figures 3(a)–(e), respectively. The band structure of the adsorption of one H on the same model is plotted in figure 3(f) for comparison. First, it can be clearly observed that the MMs of 2 μ_B per supercell for these systems originate from the two red bands in figures 3(a)–(e). Second, both the dispersion and energy level of the red bands in figures 3(a)–(e) were similar to those in figure 3(f), except for the small splitting of the two red bands near the K-point for the cases of $N = 3$ and $N = 6$. The splitting was attributed to the charge distributions for the two red bands and is discussed below.

The charge distributions for the two solid red bands in figures 3(a)–(e) at the K-point are shown in figures 4(a)–(e), respectively. The top and bottom subfigures in each panel of figures 4(a)–(e) correspond to two imbalanced states: the top subfigure had a lower energy than that of the bottom subfigure. From figures 4(a)–(d), it can be concluded that the 48 × 1-sized supercell can be divided into two segments with the H atom (p_z-vacancy) as the boundary containing short and long segments with lengths of N (3, 6, 12, and 18) and $48 - N$ units, respectively. The electrons that occupied each of the red bands were distributed on only one of the two segments, leaving the other segment empty; the electrons were evenly distributed on each atom of sublattice A within the segment. These results showed that the requirement for the antisymmetry of the wavefunction was fulfilled.

The splitting of the two red bands that appeared near the K-point for the cases of $N = 3$ and $N = 6$ was caused by the difference between the exchange energy of the short and long segments, because the exchange energy was dependent on the charge density of the involved atoms [47]. One electron was evenly distributed on each atom of sublattice A within the segment, therefore, $p_z^{\text{imbalance}}$ distributed in the short segment exhibited a lower energy than that in the long segment. The band-splitting for $N = 12$, 18, and 24 was smaller than 0.02 eV.

Figures 4(a)–(d) denote that the p_z-vacancy acted as a boundary in dividing the supercell into two segments, that is, the $p_z^{\text{imbalance}}$ charge distribution did not contain the p_z-vacancy as its center, even though $p_z^{\text{imbalance}}$ was induced by the p_z-vacancy. This also implies that $p_z^{\text{imbalance}}$ resulted from an imbalance, not an interaction. Most importantly, this led to the recombination of the p_z-orbitals in sublattice A, thereby forming individual segments for each $p_z^{\text{imbalance}}$ to rectify the imbalance.

However, for $N = 24$, the electron distribution in the supercell could not be divided into two segments. Instead, the electrons of both the red states were distributed over the entire supercell, as shown in the top and bottom subfigures of

figure 4(e). The two red bands almost degenerated, similar to that in the case of a single H atom adsorbed on a 24×1-sized graphene. We performed calculations for $N = 24$ using two different initial atomic configurations: (1) two H atoms were placed on the original graphene, and (2) one H atom was placed on the relaxed graphene with one adsorbed H atom. Both the initial configurations produced the same ground state: the total energy and MMs were similar with respect to the level of accuracy of the calculations, and the DOS and charge distribution were similar. Most importantly, the electrons of the two red bands obtained by the different initial configurations were distributed over the entire supercell, unlike for that observed for $N = 3$, 6, 12, and 18, where the electrons were distributed over one segment of the supercell, leaving the other segment empty.

The aforementioned analysis helped us to conclude that the response of the conjugated p_z-electron network to two p_z-vacancies on one sublattice was similar to that in the case of one p_z-vacancy because the origin of $p_z^{\text{imbalance}}$ was similar for one or two p_z-vacancies. The aforementioned requirements should always be fulfilled regardless of the number of p_z-vacancies appearing on one sublattice. Therefore, construction of the wavefunction for each of the two $p_z^{\text{imbalance}}$ states simply corresponded to a recombination of the p_z-orbitals in sublattice A.

This conclusion is denoted in figures 4(a)–(d); two red states ($p_z^{\text{imbalance}}$) are distributed on two individual segments without overlapping each other, as shown in the top and bottom subfigures in figures 4(a)–(d). Both the individual segments shared a common p_z-vacancy as their boundary.

The physics of magnetic ordering of the MMs in the two segments can be illustrated by figure 5. In the figure, the two segments are differentiated based on their color and black-white lobes. The up–down colors (black-gray) of the alternative lobes indicate antisymmetric wavefunctions. In principle, the wavefunction phases of the two $p_z^{\text{imbalance}}$ states should be independent, that is, the up–down colors of the lobes in the left segment could be inverted relative to the black-gray up–down order in the right segment, as shown in figures 5(a) and (b).

Let up-pink and down-green (up-black and down-gray) denote a positive phase; then, if the orbital phases on two atoms on the two sides of the p_z-vacancy (denoted by C_{left} and C_{right} respectively) were antisymmetric, as shown in figure 5(a), no electrons would accumulate on the p_z-vacancy site. Otherwise, if the orbital phases on C_{left} and C_{right} are symmetric, as shown in figure 5(b), electrons could appear on the p_z-vacancy-site. Therefore, the condition that no additional imbalance was allowed for $p_z^{\text{imbalance}}$ required the orbital phases on C_{left} and C_{right} to be antisymmetric, thereby favoring parallel alignment of the two MMs (blue arrows) on C_{left} and C_{right}. The white arrows on the other atoms in each of two segments followed the individual blue arrows, leading to all the MMs in the two segments being aligned parallel to each other because the MMs (blue and white arrows) within the same segment belonged to one electronic state, which should be parallel. In contrast, figure 5(b) shows that the two boundary atoms, C_{left} and C_{right}, had symmetric orbital phases; thus, the

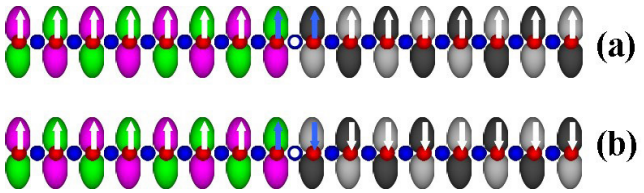

Figure 5. Schematic of the relation between the phase and magnetic ordering of two $p_z^{\text{imbalance}}$-dominant segments; the red and blue balls represent atoms of sublattices A and B, respectively; the blue ball with a white circle corresponds to the position of the p_z-vacancy; the colored and black-white lobes belong to two $p_z^{\text{imbalance}}$-dominant segments that share a common p_z-vacancy as a boundary; the colored lobes with up-pink and down-green as well as the black-white lobes with up-black and down-gray indicate positive phases; the blue arrows indicate MMs on two atoms located on two sides of the p_z-vacancy; and the white arrows are MMs on the other atoms of the segments.

MMs on the two boundary atoms (blue arrows) should have been antiparallel. For the case of $N = 24$, the MM alignment could be easily understood. The charge distributions of the two $p_z^{\text{imbalance}}$ states overlapped; thus, the MMs of one $p_z^{\text{imbalance}}$ state served as a magnetic field to induce parallel alignment of the MMs of the other $p_z^{\text{imbalance}}$ state.

Considering that the $p_z^{\text{imbalance}}$'s electron was evenly distributed on the atoms of sublattice A and there were N_{AL} and N_{AS} atoms of sublattice A within the long and short segments respectively, the two boundary atoms, C_{left} and C_{right}, contained thus $1/N_{\text{AL}}$ and $1/N_{\text{AS}}$ electrons, respectively. According to the aforementioned analysis of the orbital phases on the two boundary atoms, the coupling of the MMs in the two segments depended on the $1/N_{\text{AL}}$ and $1/N_{\text{AS}}$ electrons. The lower the p_z-vacancy concentration, the smaller will be the $1/N_{\text{AL}}$ ($1/N_{\text{AS}}$) electrons and the lower will be the exchange energy. Compared with the case of a point defect, such as graphene with vacancies, the model presented in this study represents an extreme case in which a state without decay can be realized. In the point-defect case, such as in case of graphene containing a vacancy, the charge density of a defect state can rapidly decay to a value smaller than the thermal fluctuation on the atoms of sublattice B. This difference between point-defects and straight-line-defects may explain the occurrence of controversial experimental observations [5–8].

4. Conclusions

In summary, we studied the magnetism observed in proton-irradiated graphene by constructing an extreme model of a supercell for the adsorbed of H (modeled as a straight line) onto graphene. We present a novel mechanism to explain the magnetic phenomena. This mechanism was initially suggested in our previous papers [24] and is *substantially different from conventional models* such as the Heisenberg model, the indirect exchange model, the superexchange model, the RKKY model, and the itinerant electron model [47].

We showed that the conjugated p_z-electron network in graphene plays a critical role in the spin polarization of the *sp*-electrons and magnetic ordering. The adsorption of H on

graphene saturates the p_z-orbital of C under the H atom, creating a p_z-vacancy on the conjugated p_z-electron network, thereby inducing a p_z-electron imbalance between the two sublattices of graphene. Because the $p_z^{\text{imbalance}}$ state is caused by imbalance, no further imbalance should be present and the conjugated p_z-electron network should be minimally affected for obtaining $p_z^{\text{imbalance}}$. That is, (1) the state should comprise p_z-orbitals only on the atoms of sublattice A, (2) the spatial wavefunction of the state should be antisymmetric, and (3) the state should extend over the entire crystal without any decay unless other p_z-vacancies are encountered. The spin polarization of the *sp*-electrons in graphene with a p_z-vacancy originates from the spatial antisymmetric wavefunction of $p_z^{\text{imbalance}}$ in accordance with the electron exchange antisymmetric principle.

An increase in the number of p_z-vacancies results in the creation of more $p_z^{\text{imbalance}}$ states because $p_z^{\text{imbalance}}$ *states are created by the* p_z*-orbital imbalance and not by interatomic interactions*. Although the response of the conjugated p_z-electron network to the imbalance is to create more $p_z^{\text{imbalance}}$ states, the requirement of the formation of the induced states should be satisfied, resulting in the recombination of the p_z-orbitals in sublattice A. If two p_z-vacancies exist, the electrons that fill each of two $p_z^{\text{imbalance}}$ states are not distributed over the entire crystal but are distributed in two individual segments, and the p_z-vacancies serve as boundaries. The wavefunction phase of each state should be independent although all the $p_z^{\text{imbalance}}$ states in each segment antisymmetrically comprise the p_z-orbitals of sublattice A. However, the requirements that no additional imbalance should be introduced and that the conjugated p_z-electron network should be minimally affected cause the orbital phases on the two boundary atoms, C_{left} and C_{right}, to be antisymmetric, resulting in the presence of MMs on two boundary atoms in FM alignment at a high temperature. Therefore, the spin polarization and magnetic ordering produced by our extreme model originate from the requirements for the imbalanced states.

Because $p_z^{\text{imbalance}}$ is filled by only one electron but has a long-range extent and is distributed on a $p_z^{\text{imbalance}}$-dominant segment, the MMs on each atom are considerably small and the sum of the MMs over all atoms is only one Bohr magneton (μ_B). The requirement for the imbalanced states induced by the p_z-vacancies on one sublattice leads to the MMs of all the $p_z^{\text{imbalance}}$-dominant segments exhibiting coherent FM alignment. The total MM depends on the p_z-vacancy concentration. These results explain the experimental observations of very weak magnetization at a high Curie temperature.

Acknowledgments

This work was supported by NFSC (No.61274097) and NBRPC (No. 2015CB921401).

ORCID iDs

J G Che https://orcid.org/0000-0002-9655-2760

References

[1] Esquinazi P, Hergert W, Spemann D, Setzer A and Ernst A 2013 Defect-induced magnetism in solids *IEEE Trans. Magn.* **49** 4668
[2] Han W, Kawakami R K, Gmitra M and Fabian J 2014 Graphene spintronics *Nat. Nanotechnol.* **9** 794
[3] Kheirabadi N, Shafiekhani A and Fathipour M 2014 Review on graphene spintronic, new land for discovery *Superlattices Microstruct.* **74** 123
[4] Gong C and Zhang X 2019 Two-dimensional magnetic crystals and emergent heterostructure devices *Science* **363** 706
[5] Makarova T and Palacio F (ed) 2006 *Carbon Based Magnetism: an Overview of the Magnetism of Metal Free Carbon-Based Compounds and Materials* (Amsterdam: Elsevier)
[6] Sepioni M, Nair R R, Rablen S, Narayanan J, Tuna F, Winpenny R, Geim A K and Grigorieva I V 2010 Limits on intrinsic magnetism in graphene *Phys. Rev. Lett.* **105** 207205
[7] Sepioni M, Nair R R, Tsai I-L, Geim A K and Grigorieva I V 2012 Revealing common artifacts due to ferromagnetic inclusions in highly oriented pyrolytic graphite *Europhys. Lett.* **97** 47001
[8] Nair R R *et al* 2012 Spin-half paramagnetism in graphene induced by point defects *Nat. Phys.* **8** 199
[9] Elfimov I S, Yunoki S and Sawatzky G A 2002 Possible path to a new class of ferromagnetic and half-metallic ferromagnetic materials *Phys. Rev. Lett.* **89** 216403
[10] Esquinazi P, Spemann D, Höhne R, Setzer A, Han K-H and Butz T 2003 Induced magnetic ordering by proton irradiation in graphite *Phys. Rev. Lett.* **91** 227201
[11] Červenka J, Katsnelson M I and Flipse C F J 2009 Room-temperature ferromagnetism in graphite driven by two-dimensional networks of point defects *Nat. Phys.* **5** 840
[12] Ugeda M M, Brihuega I, Guinea F and Gómez-Rodríguez J M 2010 Missing atom as a source of carbon magnetism *Phys. Rev. Lett.* **104** 096804
[13] Giesbers A J M *et al* 2013 Interface-induced room-temperature ferromagnetism in hydrogenated epitaxial graphene *Phys. Rev. Lett.* **111** 166101
[14] Wang Y, Huang Y, Song Y, Zhang X, Ma Y, Liang J and Chen Y 2009 Room-temperature ferromagnetism of graphene *Nano Lett.* **9** 220
[15] González-Herrero H, Gómez-Rodríguez J M, Mallet P, Moaied M, Palacios J J, Salgado C, Ugeda M M, Veuillen J-Y, Yndurain F and Brihuega I 2016 Atomic-scale control of graphene magnetism by using hydrogen atoms *Science* **352** 437
[16] Yazyev O V and Helm L 2007 Defect-induced magnetism in graphene *Phys. Rev.* B **75** 125408
[17] Boukhvalov D W, Katsnelson M I and Lichtenstein A I 2008 Hydrogen on graphene: electronic structure, total energy, structural distortions and magnetism from first-principles calculations *Phys. Rev.* B **77** 035427
[18] Santos E J G, Ayuela A and Sánchez-Portal D 2012 Universal magnetic properties of sp3-type defects in covalently functionalized graphene *New J. Phys.* **14** 043022
[19] Yazyev O V 2010 Emergence of magnetism in graphene materials and nanostructures *Rep. Prog. Phys.* **73** 056501
[20] Volnianska O and Boguslawski P 2010 Magnetism of solids resulting from spin polarization of p orbitals *J. Phys.: Condens. Matter* **22** 073202
[21] Fischer P and Ohldag H 2015 X-rays and magnetism *Rep. Prog. Phys.* **78** 094501
[22] Heisenberg W 1926 Mehrkörperproblem und resonanz in der quantenmechanik *Z. Phys.* **38** 411

[23] Heisenberg W 1928 Zur theorie des ferromagnetismus *Z. Phys.* **49** 619
[24] Xu W and Che J G 2019 Ferromagnetism in graphene traced to antisymmetric orbital combination of involved electronic states *J. Phys.: Condens. Matter* **31** 095801
[25] Xu W, Shang J, Yu J-X and Che J G 2019 Origin of sp-electron magnetism in graphitic carbon nitride *J. Magn. Magn. Mater.* **474** 269
[26] Pereira V M, Guinea F, Lopes dos Santos J M B, Peres N M R and Castro Neto A H 2006 Disorder induced localized states in graphene *Phys. Rev. Lett.* **96** 036801
[27] Santos E J G, Ayuela A and Sánchez-Portal D 2010 First-principles study of substitutional metal impurities in graphene: structural, electronic and magnetic properties *New J. Phys.* **12** 053012
[28] Palacios J J and Ynduráin F 2012 Critical analysis of vacancy-induced magnetism in monolayer and bilayer graphene *Phys. Rev.* B **85** 245443
[29] Sun M, Ren Q, Zhao Y, Chou J-P, Yu J and Tang W 2017 Electronic and magnetic properties of 4d series transition metal substituted graphene: a first-principles study *Carbon* **120** 265
[30] Pollmann J 1980 *Festkörperprobleme* (*Advances in Solid State Physics*) vol 20 (Vieweg: Braunschweig) p 117
[31] Kresse G and Furthmüller J 1996 Efficiency of *ab initio* total energy calculations for metals and semiconductors using a plane-wave basis set *Comput. Mater. Sci.* **6** 15
Kresse G and Furthmüller J 1996 Efficient iterative schemes for *ab initio* total-energy calculations using a plane-wave basis set *Phys. Rev.* B **54** 11169
Kresse G and Joubert D 1999 From ultrasoft pseudopotentials to the projector augmented-wave method *Phys. Rev.* B **59** 1758
[32] Blöchl P E 1994 Projector augmented-wave method *Phys. Rev.* B **50** 17953
[33] Perdew J P, Burke K and Ernzerhof M 1996 Generalized gradient approximation made simple *Phys. Rev. Lett.* **77** 3865
[34] Castro Neto A H, Guinea F, Peres N M R, Novoselov K S and Geim A K 2009 The electronic properties of graphene *Rev. Mod. Phys.* **81** 109
[35] Kuzemsky A L 2013 Unconventional and exotic magnetism in carbon-based structures and related materials *Int. J. Mod. Phys.* B **27** 1330007
[36] Rafique M, Shuai Y, Tan H-P and Muhammad H 2017 *Appl. Surf. Sci.* **408** 21
[37] Rafique M, Unar M A, Ahmed I, Chachar A R and Shuai Y 2018 *J. Phys. Chem. Solids* **118** 114
[38] Feng Y P, Shen L, Yang M, Wang A, Zeng M, Wu Q, Chintalapati S and Chang C-R 2017 Prospects of spintronics based on 2d materials *WIREs Comput. Mol. Sci.* **7** e1313
[39] Náfrádi B, Choucair M and Forró L 2017 Electron spin dynamics of two-dimensional layered materials *Adv. Funct. Mater.* **27** 1604040
[40] Katsnelson M I 2012 *Graphene: Carbon in Two Dimensions* (Cambridge: Cambridge University Press)
[41] Singh R 2013 Unexpected magnetism in nanomaterials *J. Magn. Magn. Mater.* **346** 58
[42] Pereira V M, Lopes dos Santos J M B and Castro Neto A H 2008 Modeling disorder in graphene *Phys. Rev.* B **77** 115109
[43] Kittel C 2004 *Introduction to Solid State Physics* 8th edn (New York: Wiley)
[44] Griffiths D J 2016 *Introduction to Quantum Mechanics* 2nd edn (Cambridge: Cambridge University Press)
[45] Muhammad R, Shuai Y, Irfan A and He-Ping T 2018 *RSC Adv.* **8** 23688
[46] Muhammad R, Shuai Y, Irfan A, Shaikh R and Tunio M A 2019 *Appl. Surf. Sci.* **480** 463
[47] Mohn P 2003 *Magnetism in the Solid State: an Introduction* (Berlin: Springer)